Particle
& Particle Systems Characterization
www.particle-journal.com

Materials Views
www.MaterialsViews.com

$Cd_xHg_{(1-x)}Te$ Alloy Colloidal Quantum Dots: Tuning Optical Properties from the Visible to Near-Infrared by Ion Exchange

Shuchi Gupta, Olga Zhovtiuk, Aleksandar Vaneski, Yan-Cheng Lin, Wu-Ching Chou, Stephen V. Kershaw, and Andrey L. Rogach*

The energy gap between valence and conduction levels in colloidal semiconductor quantum dots can be tuned via the nanoparticle diameter when this is comparable to or less than the Bohr radius. In materials such as cadmium mercury telluride, which readily forms a single phase ternary alloy, this quantum confinement tuning can also be augmented by compositional tuning, which brings a further degree of freedom in the bandgap engineering. Here it is shown that compositional control of 2.3 nm diameter $Cd_xHg_{(1-x)}Te$ nanocrystals by exchange of Hg^{2+} in place of Cd^{2+} ions can be used to tune their optical properties across a technologically useful range, from 500 nm to almost 1200 nm. Data on composition-dependent changes in the optical properties are provided, including bandgap, extinction coefficient, emission energy and spectral shape, Stokes shift, quantum efficiency, and radiative lifetimes as the exchange process occurs, which are highly relevant for those seeking to use these technologically important QD materials.

1. Introduction

There have been a number of studies on the use of ion exchange, both cationic and anionic, in colloidal quantum dots (QDs) to bring about compositional change.[1–8] Modification of the internal structure, e.g. formation of heterostructures due to localized distribution of the exchanged species, or even localised morphology changes due to the preference of the incoming species for a different structure, e.g., zincblende vs. wurtzite can be expected during the exchange, and defects may also be introduced at the internal boundaries between the old and new phases. The ion exchange method is a useful tool to build nanoparticle structures that may be synthetically difficult by more direct approaches, by using the starting material as a template into which the desired ions are introduced after the nanoparticle size and shape have been established.

By controlling the degree of ion exchange it is in principle possible to form quantum dots with controlled alloy compositions. This is especially useful for the $Cd_xHg_{(1-x)}Te$ ternary alloy system where Cd^{2+} and Hg^{2+} have almost identical ionic radii and in the respective zincblende lattices, the parent CdTe and HgTe lattice constants differ by only 0.3% (6.482 Å and 6.462 Å, respectively).[9] This remarkably convenient property has been extensively exploited in bulk $Cd_xHg_{(1-x)}Te$ semiconductor technology to produce highly engineered optical components, in particular infrared (IR) and far IR photodetectors.[10] The material's bandgap may be tuned continuously from near zero (due to the fact that bulk HgTe is a semi-metal),[9] to that of pure CdTe (around 1.44 eV at room temperature)[9] while the structure remains zincblende.

We have studied CdTe and HgTe nanoparticles extensively[11–13] and have previously reported the fact that when attempting to produce HgTe/CdTe multilayer nanoparticles, it appeared that alloying of the cations was occurring to some degree instead.[14] Recently others have studied the $Cd_xHg_{(1-x)}Te$ system in more detail, Taniguchi and others[15,16] having shown ion exchange in CdTe QDs in organic solvent media and Lesnyak et al.[17] and Sun et al.[18] demonstrating direct synthesis of alloyed $Cd_xHg_{(1-x)}Te$ QDs. Moon et al.[19] have extensively reviewed the literature on ion exchange in nano and mesoscale particles, wires and other types of structures and have classified the types of exchange process into four main categories: alloy formation, galvanic replacement, cationic and anionic replacement. Many of the works that are cited by Moon were on larger scale structures that are easier to characterize, e.g., by HRTEM, but this is considerably more difficult for small (typically, 2–4 nm in diameter) QD particles and complicated by the lack of strong contrast between the Cd^{2+} and Hg^{2+} ions. Yang et al.[20] have also studied the alloying process in CdTe QDs by doping with Hg^{2+} ion solutions, but adopted a different methodology to the one cited here. They studied the exchange process with CdTe starting solutions that were either precipitated and re-dissolved

S. Gupta, O. Zhovtiuk, A. Vaneski, Dr. S. V. Kershaw, Prof. A. L. Rogach
Department of Physics and Materials Science & Centre for Functional Photonics (CFP)
City University of Hong Kong
Hong Kong S.A.R
E-mail: skershaw@cityu.edu.hk
Dr. Y.-C. Lin, Prof. W.-C. Chou
Department of Electrophysics
National Chiao Tung University
Hsinchu, 30010, Taiwan, R.O.C.

DOI: 10.1002/ppsc.201200139

prior to use or were used as synthesised. In the former case excess cadmium ions and excess ligand were removed, while in the latter case, probably 60% or so of the Cd^{2+} starting ion concentration would have remained in solution along with an excess of stabilizer. In the former case their exchange process led to the formation of Cd_x Hg_{1-x} Te nanowire networks, while the un-precipitated case led to isolated alloy QDs. In the present case we took care to remove excess cadmium ion and stabilizer used in the synthesis, but the mercury ion added during our exchange process was stabilized at high pH (>10) with mercaptopropionic acid. This was prepared with the doping solution at high pH before the addition of the metal salt to avoid reduction of the latter and resulted in a clear doping solution, with no reduction of mercury (II). The resulting alloy QDs also benefited from the early restoration of a complete layer of thiolate stabilizer molecules at the surface, promoting the formation of alloy QDs over the formation of nanowires, a feature also evident in the fact that the photoluminescence remained observable and recovers to a level comparable with the starting material, in contrast to earlier observations.

In this paper we have systematically studied the ion exchange of Hg^{2+} in place of Cd^{2+} in 2.3 nm diameter CdTe nanoparticle starting material with the exchange carried out in aqueous solution. Starting with CdTe particles emitting in the visible (at 541 nm) we are able shift the emission out to 1166 nm in the near IR. Such an approach bridges the upper wavelength range for CdTe nanocrystal emission and the lower wavelength range for HgTe QDs. This is an especially interesting range for solar energy technology (e.g., wider absorption range panchromatic QD absorbers[21] and luminescent QD solar concentrators[22,23] closely tuned to the silicon band edge at around 1.3 eV), and a few other applications such as biolabelling in the near-IR to access transparency windows in tissues, including both in vitro and in vivo low background noise fluorescent labelling of tumour structures.[24,25] We describe the changes in the optical properties: bandgap (E_g); extinction coefficient; emission energy and spectral shape; Stokes shift; quantum efficiency; and radiative lifetimes as the exchange process occurs, and correlated with compositional analysis. By following changes over an extended time and at a range of temperatures we also observe the kinetics of the exchange processes on short (mins to a few hours) and longer timescales which are consistent with a fast initial uptake of Hg^{2+} at the surface of the CdTe particles, followed by a gradual interdiffusion of the two cations.

As shown in **Figure 1**a, in the bulk Cd_x $Hg_{(1-x)}$Te ternary system, E_g is almost linearly dependent on the composition factor, x. For 2.3 nm diameter nanoparticles, the endpoints for pure HgTe ($x = 0$) and CdTe (x = 1) QDs are both blue-shifted relative to respective bulk materials, with the shift being greater for HgTe than CdTe. At 2.3 nm, HgTe QDs are more tightly confined than CdTe with their Bohr radii being 27 nm and 5 nm respectively (using data from ref. [6]. Using the relationship, $r_B = r_o \in_r \frac{m_o}{\mu}$, where r_o is the atomic Bohr radius, m_o is the free electron mass, and μ is the exciton effective mass in units of m_o, along with data for the permittivity ε_r and μ derived from the literature[26–28] shown in Figure 1b, Bohr radii can be calculated for composition values from $x = 0$ to $x = 1$. It should be pointed out that, since the exciton reduced mass, μ, has a very small value in the vicinity of the semi-metal to semiconductor transition near

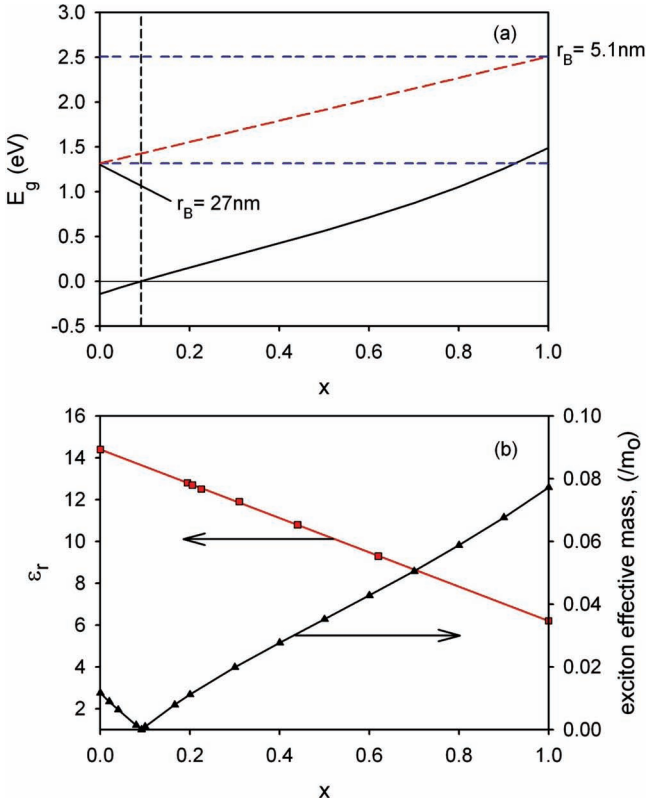

Figure 1. a) The bulk $Cd_xHg_{(1-x)}Te$ alloy bandgap (heavy black curve) is an almost linear function of composition (x). The room temperature $E_g(x)$ curve shown here is calculated from Nemirowsky et al.[30] For QDs of 2.3nm diameter used in this study, the end points ($x = 0$ and $x = 1$) are blue shifted, and in the case of pure HgTe nanoparticles, the material becomes a semiconductor rather than a semi-metal. Varying the composition allows bandgap energy tuning between the horizontal dashed lines, however the exact tuning relationship is probably not linear as shown by the straight dashed red line joining the two end points. b) Compositional dependence of the relative dielectric constant and the exciton effective mass for $Cd_xHg_{(1-x)}Te$. The electron effective mass (and consequently the exciton effective mass) is very small in the vicinity of the semi-metal–semiconductor transition. Data are derived from ref. [27,30] and the hole effective mass is taken as constant at $0.44m_o$. See Supporting Information for further details.

$x = 0.092$ (at 300 K) this leads to a rapidly diverging value for r_B implying very strong confinement. For 2.3 nm diameter QDs, the confinement is strong even in the CdTe starting material ($r_B = 5$ nm) and in pure HgTe 2.3 nm nanoparticles, r_B is 27 nm. For this reason, simple bandgap models such as the particle in a box approximation are highly inaccurate and tight binding calculations[29] are a more appropriate approach. This makes theoretical estimation of any bowing parameter more difficult, but even from the (inaccurate) particle in a box model it can be seen that, while the bulk Cd_x $Hg_{(1-x)}$Te alloy bandgap curve is near linear, as the (dominant) confinement energy term scales as $1/\mu$, for compositions in the vicinity of $x = 0.092$ where the exciton effective mass is very small, a departure from linearity for $E_g(x)$ may be expected.

As already mentioned, when the ion exchange process is carried out we may not necessarily obtain the simple $Cd_xHg_{(1-x)}Te$

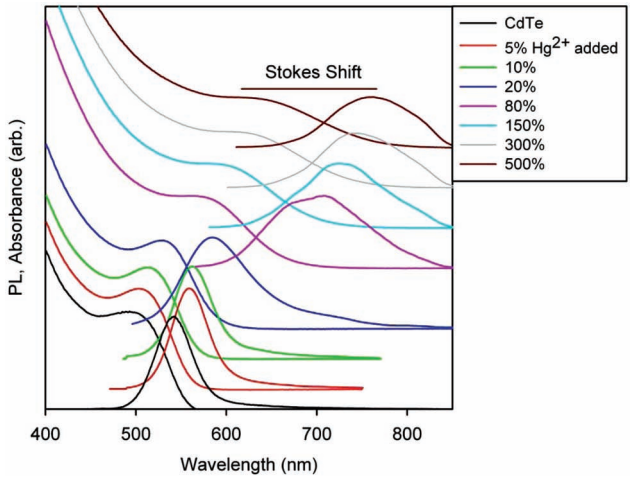

Figure 2. Absorption and PL spectra (excitation wavelength 400 nm) of $Cd_xHg_{(1-x)}Te$ nanocrystals measured 30 mins after addition of various amounts of Hg^{2+} ion relative to the initial Cd^{2+} content in CdTe QDs. Relative to the CdTe starting material, absorption edges and PL peaks shift to the red, and PL spectra progressively broaden with increasing Hg^{2+} dose. Individual PL and absorption spectra have been vertically shifted and scaled for clarity. During the exchange process and with increasing Hg^{2+} dose, the exciton and emission peaks of $Cd_xHg_{1-x}Te$ QDs shift to longer wavelengths at different rates and so the Stokes shift changes with QD composition.

structure with metal ions evenly distributed throughout the particles.[31] One or other cation may stay preferentially at the surface, the particle size distribution may change (e.g., by later re-adsorption of ejected Cd^{2+} ions) or other competing exchange process may occur. These may further complicate the interpretation of the $E_g(x)$ behavior and make unequivocal experimental determination of the bowing curve for the case of a homogeneously alloyed QD difficult.

2. Results

2.1. Evolution of PL and Absorption Spectra for Samples at Room Temperature

Figure 2 shows a typical set of absorption and emission spectra for the set of different Hg^{2+} dose samples, in this case measured 30 mins after addition of the Hg^{2+} solution and with the samples maintained at room temperature. In order to more clearly show the spectra on the same plot both absorption and emission spectra have been arbitrarily shifted and rescaled. The excitonic peak in the absorption spectrum shifts to longer wavelength with Hg^{2+} dose. This peak also becomes less pronounced, eventually becoming more of an inflexion than a recognizable peak. In these cases the second derivative of the curves was used to determine the location of the bandgap. Emission spectra also shift to longer wavelengths (for examples of >1000 nm emission see Supporting Information Figure S1), but at a different rate in general than the absorption peaks (inflexion points) hence the Stokes shift separating the two features also changes during the exchange process. If the Stokes shift had remained constant of course, the PL peak position would have been a more distinct feature to use to estimate the bandgap, however this was not the case and so absorption spectra remain the only option despite the excitonic feature associated with the band edge becoming less distinct.

Sets of data such as shown in Figure 2 were collected at time intervals for a set of solutions (Hg^{2+} dose = 5% to 500%) stored at room temperature over a period of several days and absorption peak wavelength and intensity, and emission peak wavelength were extracted from the spectra. Supporting Information Figure S2a shows the complete trend for the absorption wavelengths corresponding to the lowest exciton energy level for each sample. At long times, the high Hg^{2+} dose samples start to saturate (i.e., there is little difference in the wavelength reached), though theoretically a longer maximum wavelength of ≈1043 nm[32] might be expected for a simple $Cd_xHg_{(1-x)}Te$ alloy composition QD with no change in size. The corresponding data for the emission peak wavelengths obtained from the set of fluorescence spectra are shown in Supporting Information Figure S2b. Again the overdosed samples tend to level out at longer times where exchange is probably closer to saturation.

2.2. ICP–AA Nanocrystal Concentration Measurement

The concentration of the nanoparticles in the exchange solutions, and the CdTe starting material were measured by ICP-AA after 26 h. Samples were first precipitated and washed by adding methanol, and the dried precipitates were dissolved in dilute aqua regia to give clear solutions of metal and tellurium salts. These were diluted further before measurement. Typical metal ion concentrations of 0.163 mM/L were measured, corresponding to QD concentrations of around 1.2 uM/L.

2.3. Extinction Coefficients of $Cd_xHg_{(1-x)}Te$ Alloy QDs and Determination of Composition

The variation of the intrinsic absorption coefficient with bandgap energy, derived from exciton peak positions is shown in **Figure 3**. The coefficient values are calculated from absorption spectrum intensity data (at 405 nm) taken from the same sets of spectra shown in Supporting Information Figure S2a. Following the approach used by Hens et al. for CdTe, PbSe and PbS QDs,[33–35] short wavelength optical density data and Cd ion concentrations are combined to calculate extinction coefficient values and thence intrinsic absorption coefficients. Optical density (OD) data were taken at 405 nm, where Maxwell Garnett effective medium theory can be taken to be valid and allowing comparison with theoretically calculated data from the complex permittivities of the bulk semiconductor and host solvent medium. Experimental values for the CdTe starting material were 85 350 cm^{-1}, compared with 82 677 cm^{-1} calculated from literature data for bulk CdTe, and approximately 75 500 cm^{-1} (at 410 nm) calculated by Kamal et al.[33] Figure 3 also shows the calculated value (vertical red dashed line) for pure HgTe. This was calculated from experimental absorption cross-section data from Lhuillier et al.[36] Values at intermediate compositions (x) from all sample series (different Hg^{2+} doses and measured at

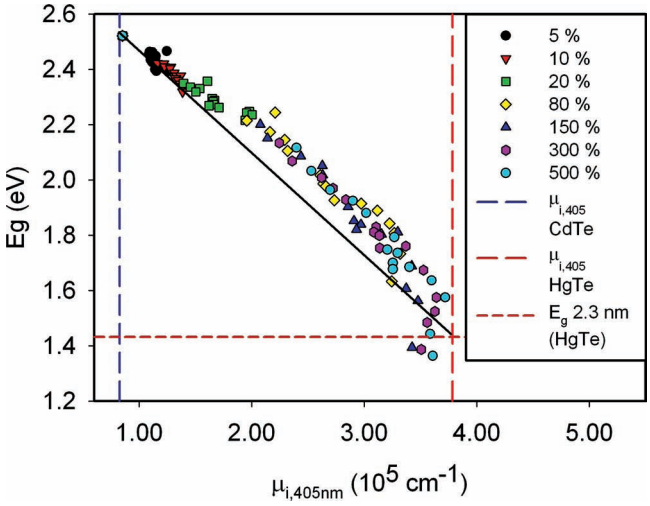

Figure 3. Bandgap energy vs. intrinsic absorption coefficients derived from optical density measurements at 405 nm ($\mu_{i,405nm}$) for alloy samples over a range of times and for samples prepared with various Hg^{2+} doses. The vertical blue dashed line indicates the intrinsic absorption coefficient for pure CdTe 2.3 nm diameter dots calculated from bulk CdTe data.[33] For comparison with the complete exchange case ($x = 0$) approximately the same size (2.3 nm) HgTe QDs were grown (see Supporting Information Figure S3). The red vertical dashed line is the corresponding value for pure HgTe derived from the absorption cross section of Lhuillier et al.[36] The horizontal red dashed line is the estimated bandgap for 2.3 nm HgTe QDs calculated from PL data,[32] assuming a Stokes' shift of 150 nm. The intersection of the horizontal and vertical red dashed lines is estimated to be the extremum for pure HgTe. The composition, x, of $Cd_xHg_{1-x}Te$ can be determined from the measured intrinsic absorption coefficients, relative to the span between the CdTe and HgTe limiting values.

different times) were calculated from measured OD values, and correlated with bandgap energies.

The composition, x, (making no assumptions about the uniformity of the distribution of cations) can be calculated from the extinction coefficient values using, $x = \frac{(\mu_{i,405\,nm}(x)-\mu_{i,405\,nm}(x=1))}{(\mu_{i,405\,nm}(x=0)-\mu_{i,405\,nm}(x=1))}$, i.e., from the relative intrinsic absorption coefficient position between the CdTe and HgTe limits.

The excitonic peaks in the absorption spectra become progressively broader and "washed out" as the exchange process proceeds (Figure 2). This makes accurate determination of bandgap energies progressively more difficult resulting in greater scatter in Figure 3 for lower bandgap compositions. Where no clear absorption peak was observed, second derivatives of absorption spectra were calculated and the inflexion point taken as the location of the bandgap.

Between the CdTe and HgTe limits, the bandgap vs. extinction coefficient curve is essentially a bowing curve. The end points (pure CdTe and pure HgTe) are respectively the intersection of the data points and the vertical blue curve, and the intersection of the horizontal and vertical red dashed lines. It is immediately clear that the data appears to bow above the straight line joining the two extrema, rather than below it. This would be consistent with a non-homogeneous distribution of the two cations, with an increasing Cd^{2+} ion concentration gradient towards the centre of the QDs. This would tend to give more inflated bandgap energies than for the evenly distributed cation case, making the curve appear higher until Hg^{2+} concentrations start to saturate and a gradient can no longer be accommodated. Nonetheless values for the net composition may still be determined, though the data suggests that a gradient core-shell (CdTe rich core) is formed initially and at lower Hg^{2+} doses.

Many bulk ternary alloy systems show bandgap vs. composition curves which are not quite linear, and mostly parabolic to some degree, even though their lattice parameters have a linear composition dependence in accordance with Vegard's law. However Protière and Reiss[37] have shown that this deviation is often not very pronounced in QD alloys where the anion is common between the two constituent binary systems. Attempts have been made to relate the so-called bowing parameter characterising the deviation from linearity to the difference in the electronegativities of the two end components,[38] here CdTe (0.41) and HgTe (0.1).[9] Wei et al.[39] investigated the optical bowing of bulk ternary cadmium chalcogenide alloys where the metal ion is common and the chalcogen ratio varied.

In practice, with QD ternary materials the apparent bowing behavior as determined here is further complicated by size and compositional (variation in x) polydispersity and also the spatial distribution of the Cd^{2+} and Hg^{2+} ions throughout the QDs. In this case our data seem consistent with some degree of a composition gradient at least until the exchange of Cd^{2+} and Hg^{2+} ions is near complete. Without detailed elemental mapping or ultra high resolution TEM of individual nanoparticles (both of which are difficult with such small nanoparticles, and similar metal ions) this is indirectly inferred. It is of course implicitly assumed that exchange is not accompanied by any change of QD size, however further growth would tend to depress rather than increase the bandgap energy due to reduced confinement. Nevertheless, it would of course be helpful to accurately verify the diameter constancy, but that is very difficult by TEM with such small aqueous QDs which tend not to disperse evenly on the microscopy grids making clear direct diameter determination problematic.

The existence of composition gradients in small QDs (both III-V and II-VI materials) synthesized in organic solvents has been successfully studied by several groups using a controlled etching method coupled with ICP-AA analysis of the supernatant material at various etch times. For example Beberwyk et al.[40] used the technique to follow In, Cd and Ga profiles in pnictide QDs. They ensured good accuracy, washing their materials by several (typically 3 or more) successive rounds of precipitation and re-dissolution prior to the etching study to completely remove excess metal precursors not converted to QDs during their synthesis. Yu et al.[41] used a similar etching/ICP-AA technique in their work on CdTe, and CdSe materials and also emphasized the need to ensure that all excess free metal ions are removed prior to the analysis. However this is somewhat difficult for thiol stabilized QDs grown in water. We found that after the first round of precipitation of the alloy QDs it was not possible to precipitate them a second time (at least not on a timescale rapid enough to be suitable for our time dependent studies i.e. fast enough that the compositions or gradients would not have changed significantly). In organically grown QDs this problem is not encountered; several successive precipitation cycles can readily and rapidly be carried

out. Removal of free metal ions is even more necessary in ion exchange studies where a large excess concentration of the displacing metal ion is used. Sun et al.[18] have used the controlled etching/ICP-AA technique to probe the Cd content of directly grown (one pot synthesis) $Cd_xHg_{1-x}Te$ alloy QDs grown in water, but it is not clear if they were able to do repeated cycles of precipitation to wash out the free metal beforehand. In their case they saw a very large apparent drop of the Cd concentration at the outset of their etching profiles, cadmium being a far more water soluble ion than mercury and incorporated into the QDs at concentrations far lower than the ratio of metals used in the synthesis.

3. Discussion

3.1. Stokes Shift and Phonon Emission in $Cd_xHg_{(1-x)}Te$ Alloy QDs

As seen in Figure 2, during the exchange process and with increasing Hg^{2+} dose, the exciton and emission peaks of $Cd_xHg_{1-x}Te$ QDs shift to longer wavelengths at different rates and so the Stokes shift changes with QD composition as shown in **Figure 4**. For comparison, Figure 4 also shows a value for pure HgTe QDs ($x = 0$) of approximately the same size, representing the end point for 100% exchange (see Supporting Information Figure S3). As x decreases from 1, at intermediate concentrations there is a significant departure from a linear trend for the Stokes shift as a function of the composition. At low x values (approaching saturation with Hg^{2+}) the deviation starts to reduce as the case for pure HgTe QDs is approached. Again the intermediate range deviation may be an indication of a cation composition gradient.

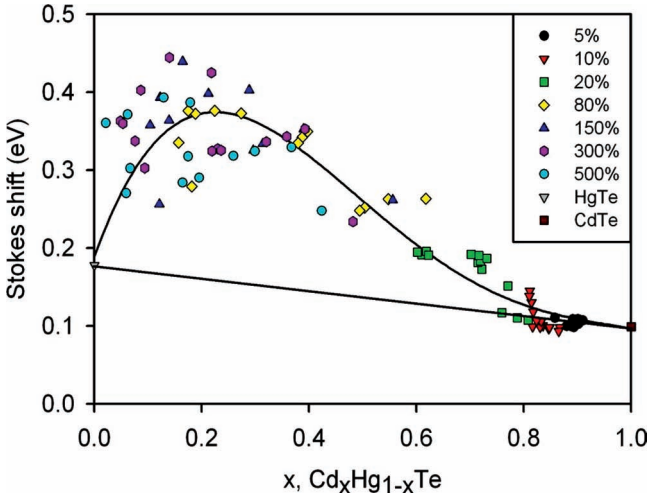

Figure 4. Stokes shift (in eV) vs. the average composition, x, of 2.3 nm $Cd_xHg_{1-x}Te$ QDs. Several samples treated with various concentrations of Hg^{2+} solution (as indicated) were tracked over a period of time as the ion exchange proceeded. Also shown for reference is a point at $x = 0$ for pure HgTe QDs of the approximately the same size, synthesised separately (see Supporting Information Figure S3), and a point for the CdTe starting material ($x = 1$). The latter points are joined by a straight line and a simple polynomial fit through the scattered points (with the end points highly weighted) as a guide to the eye.

The Huang Rhys parameter,[42] S, at room temperature, can be estimated from our Stokes shift data and literature values for LO phonon energies and is a measure of the number of phonons that must be emitted after excitation at absorption energy, E_g, and subsequent radiative relaxation. It is also interpreted as a measure of the electron-phonon interaction strength, with values >10 typically indicating strong interactions.[43] S can be experimentally determined as, $S = 1/2\left(\frac{\Delta E}{\hbar\omega} + 1\right)$, where $\hbar\omega$ is the energy of the (LO phonon) vibrational quanta and ΔE the Stokes shift. Dzhagan et al.[44] have compared bulk CdTe LO phonons energies with those in 4.5 nm diameter QDs at 50 K and room temperature. They observed values of 168 cm^{-1} (50 K) and 158 cm^{-1} (298 K) (20.9 meV and 19.6 meV) respectively compared with values ranging from 170 cm^{-1} to 173 cm^{-1} (21.1 meV to 21.5 meV) for the bulk CdTe material. This indicates a relatively weak confinement effect on the phonon energy, at least for larger CdTe QDs. Here we measure a Stokes shift of 0.227 eV for CdTe, giving a value for S of just under 6 at room temperature.

We are not aware of any reports of the phonon structure or frequencies of $Cd_xHg_{1-x}Te$ alloy QDs to date, but the nature of optical phonons in the bulk material has been extensively studied (see references in the review by Dornhaus and Nimtz[45]). The situation is a little more complicated than that in pure CdTe, with two mode behavior (simultaneous CdTe-like and HgTe–like) for LO and TO phonons alike. Baars and Sorger[26] give values for the higher energy (CdTe-like) LO phonon frequency at 300 K as a function of x, with a near linear trend following where ω_{LO} is in cm^{-1} and x is the usual composition parameter.

This range corresponds to phonon energies extending from just under 20.8 meV (CdTe) down to 18.4 meV (HgTe). For our QD material the effects of confinement may be greater than for the 4.5 nm diameter CdTe studied by Dzhagan et al.,[44] as quantum confinement is greater in our smaller particles, and the Bohr radius increases as the Hg^{2+} content increases. However, as an approximate estimate, if we take the value for the bulk CdTe-like LO phonon energy at $x = 0.3$ as 19 meV and a Stokes shift of 0.51 eV, then the Huang Rhys parameter where the Stokes shift is greatest is just under 14. Properly accounting for the effect of confinement on the phonon energies will increase these S values slightly. It is instructive to compare the Stokes shift vs. concentration curve with the curve for the electron effective mass (Figure 1b). We note that the maximum in the Stokes shift occurs in the concentration range where the electron effective mass is small.

3.2. PL Quantum Efficiency and Lifetime During and After Exchange

The ion exchange process must inevitably involve some disruption to the QD surface. Bonding with surface ligands must be temporarily disrupted as well as the cations exchanging position, both influencing the PL QE of the QDs. In addition the internal distribution of the cations initially may not be homogeneous, further affecting efficiencies. The QEs of the room temperature samples introduced above were derived from the absorption and emission spectra as previously described and

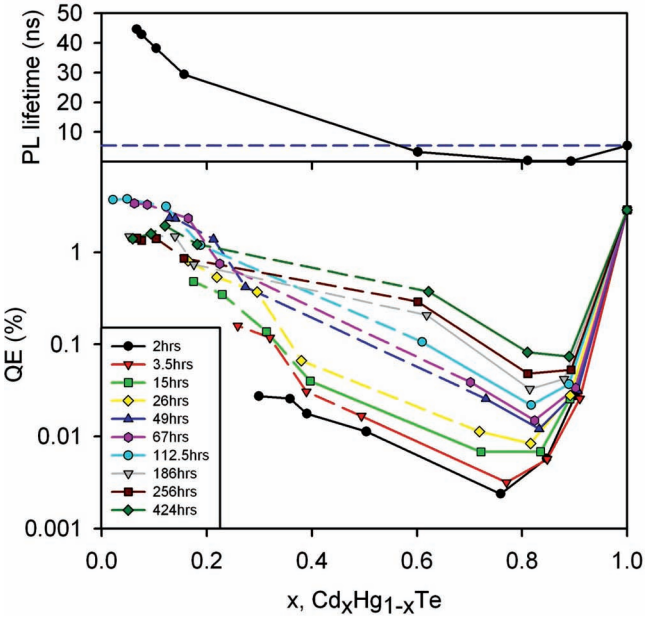

Figure 5. PL quantum efficiencies of $Cd_xHg_{(1-x)}Te$ nanocrystals vs. concentration, *x*. To allow the trends to be more clearly seen, a logarithmically scaled QE axis has been used. The upper graph shows PL radiative lifetime measurements for the same materials measured at around 256 h. Here the lifetime for the CdTe starting material is shown as a horizontal dashed blue line. Normalized radiative decay curves were fitted to a stretched exponential form: $I(t)/I_o = e^{-(t/\tau)\beta}$, where β is a stretch parameter (ranging from 0.44 to 0.84 for the 5% and 500% Hg^{2+} samples respectively) and τ is the decay time.

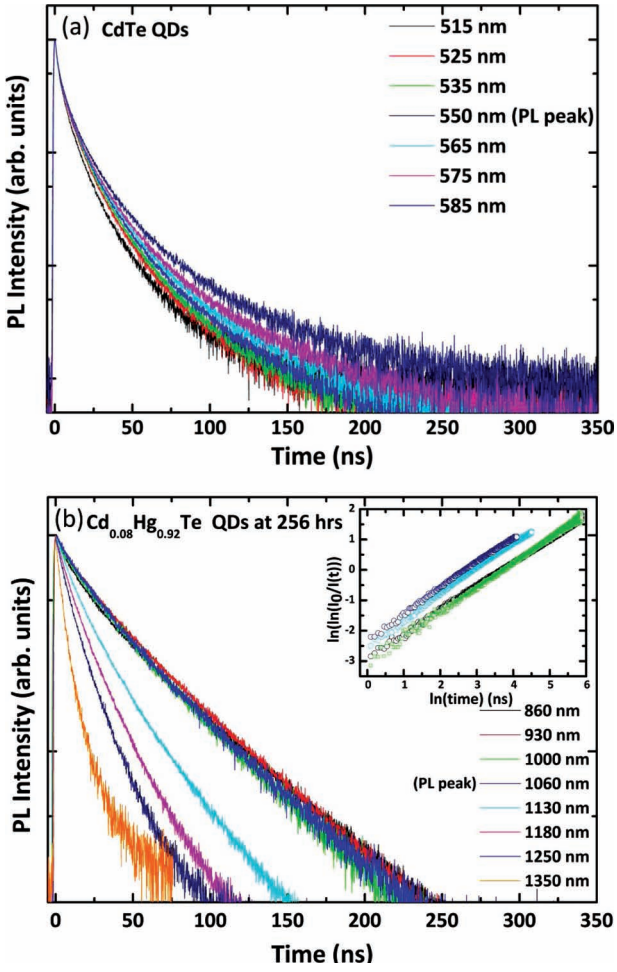

Figure 6. Normalized time resolved PL decay curves for a) pure CdTe QDs and b) $Cd_{0.08}Hg_{0.92}Te$ QDs. Measurements were made at wavelengths corresponding to the peak of the emission spectrum and at wavelengths on either side of the peak in each case, as indicated. Decay times (and stretch factors) derived from this data are emission wavelength dependent for all samples. The inset in (b) shows decay curves in ln(ln) vs. ln format spanning up to 5 orders of the factor e in some cases and illustrates the excellent fitting to the stretched exponential form over a large range.

these are shown in **Figure 5** as a function of the concentrations as derived from Figure 2. For comparison, PL lifetimes were measured in the later stage of the exchange process at around 256 hours. The PL radiative decay curves were fitted to stretched exponential decay functions characterised by a lifetime, τ, and a stretch parameter, β. The dependence of both parameters upon the initial Hg^{2+} dose closely reflects the trend in the samples' QEs by this point in time. The lifetime is an indicator of both composition; higher Hg^{2+} concentration nanocrystal materials tend to have longer lifetimes than CdTe QDs, and also the quality of the QD materials, particularly the extent of surface defects, is improved. The extent of surface damage and its eventual recovery in the later stages can be followed in the series of QE curves over time. Initially there is over two orders of magnitude reduction in PL efficiency relative to the QE of the freshly precipitated CdTe QD master batch. The removal of excess Cd^{2+} ion left from the synthesis of the CdTe QDs, by precipitation and re-dissolution prior to starting the ligand exchange had already caused some (much smaller) reduction in its QE, though over the next three days the QE of the CdTe starting material showed some recovery (from 2.9% to 6.2%). After somewhere between 30 and 70 min the ion exchange samples start to recover, with the higher Hg^{2+} dose samples recovering fastest and to the greatest extent. The three most highly dosed samples briefly exceed the CdTe starting QE before declining a little at the longest times. During the storage time, the materials were all held at room temperature and in contact with the Hg^{2+}/MPA doping solution. The recovery phenomenon after other types of QD ion exchange reactions has also been widely observed by others. Alivisatos's group[46] observed recovery in CdS nanorods, CdSe QD doped CdS nanorods, and also Cu doped versions of the later and they were able to elucidate the relative contributions of surface defects, internal stacking faults and low level Cu impurities in their case, to the initial drop in QE.

3.3. Time Resolved PL Spectra

In addition to measuring the PL lifetimes at the emission peak wavelengths shown in Figure 5 above, we also measured the lifetimes at a number of other wavelengths either side of the emission peaks for each sample, as shown in **Figure 6**a,b for pure CdTe and for an $x = 0.08$ $Cd_xHg_{(1-x)}Te$ sample. PL decay

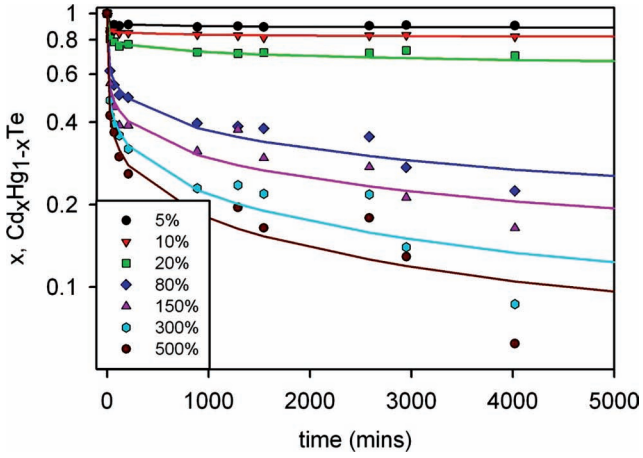

Figure 7. Kinetics of the concentration parameter, *x*, vs. exchange time for several samples treated with different Hg^{2+} concentrations. The shift in the composition over time is compared for several solutions, each doped with Hg^{2+} salt solutions at the indicated concentrations relative to the original amount of Cd^{2+} ion.

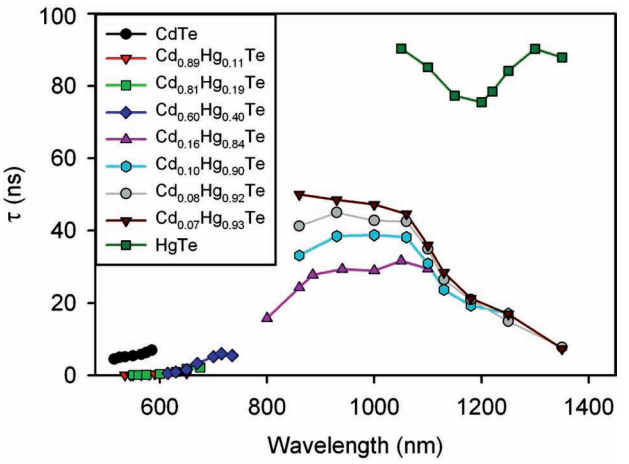

Figure 8. Spectral variation of time resolved PL lifetimes for each of the room temperature cation exchange $Cd_xHg_{(1-x)}Te$ QD samples (after 256 h), as well as the CdTe QD starting material and pure HgTe QDs of a similar size for reference (see Supporting Information for synthesis details).

curves were again fitted to stretched exponential decay processes. The trends in the spectrally resolved lifetimes for each sample, and for pure CdTe and HgTe QDs also, are explored further below.

3.5. Kinetics of the Cation Exchange in $Cd_xHg_{(1-x)}Te$ Alloy QDs

The kinetics of the exchange process(es) in $Cd_xHg_{(1-x)}Te$ alloy QDs, i.e., concentration, *x*, as a function of the exchange duration is shown in **Figure 7**. The log–linear plot clearly indicates very different rate constants at short and longer timescales. This is consistent with a fast surface cation exchange (displacement of Cd^{2+} by Hg^{2+}) taking anything up to 2 h, followed by a much slower interdiffusion of the new Hg^{2+} surface ions into the interior of the QDs over tens to several hundred hours at room temperature. Further support for the latter stage hypothesis is shown in Supporting Information Figure S4. In this case aliquots were removed from an ion exchange solution at 60 min and at 150 min. Each of these aliquots were precipitated using iso-propanol to remove excess Hg^{2+} ions (and any displaced Cd^{2+} ions) not already absorbed into the QDs and the exciton peak wavelengths of all three solutions were measured at further time intervals. The removal of free metal ions did not halt or materially alter the rate at which the peak continued to shift (relative to the untreated material), implying that exchange of cations across the surface had already almost ceased and that the continuing shift was due to internal interdiffusion of the two metal ions, Cd^{2+}/Hg^{2+}.

3.6. The Wavelength Dependence of Spectrally Resolved Lifetimes

Van Driel and co-workers[47] have considered the theoretical emission frequency (and hence size) dependence of QD spontaneous emission rates. For strongly luminescent CdSe and CdTe nanoparticles they observe lifetimes of the order of 25 ns (for 620 nm emitting 6.5 nm CdSe) and a supralinear increasing relationship between decay rate and emission frequency. Their tight binding model predicts a linear dependence, with values around 30% higher than they observe in the QD size range covered.

Spectrally resolved fluorescence lifetimes for each of the 7 room temperature cation exchange $Cd_xHg_{(1-x)}Te$ QD samples are shown in **Figure 8** along with the corresponding data for the CdTe QD starting material and a sample of HgTe QDs of a similar diameter. For the CdTe starting material the lifetimes vary far less with emission wavelength than the higher (>20%) Hg^{2+} content alloy samples, and increase slightly with increasing wavelength, with the stretch parameter remaining fairly constant. By comparison, at 80% added Hg^{2+} the alloy sample has already a longer lifetime than CdTe QDs on the short wavelength side of its emission and this increases slightly towards the peak emission wavelength. At wavelengths beyond the emission peak for the higher Hg^{2+} content samples the lifetime falls with increasing wavelength. The longer lifetime decays are more mono-exponential in nature, but less so away from the emission peaks. For pure HgTe QDs the lifetimes are higher, averaging around 80ns and in this case the curve shows a slight dip in the vicinity of the peak emission wavelength.

We have shown earlier (Figure 5), and as van Driel et al. point out,[47] the emission lifetime is strongly dependent on the surface state (and material quality in general) of the colloidal QDs. Generally, less than perfect crystallinity or surface passivation is accompanied by strong non-radiative emission[48] leading to shorter lifetimes than the theoretical ideal. One possible explanation for a decreasing lifetime with increasing emission wavelength might be that larger particles have relatively lower quantum efficiency than smaller particles, and that the disparity between the two becomes greater as the Hg^{2+} content is increased. Experimentally (Figure 5), measured lifetimes

closely follow the material's QE, i.e., batches of a given material with a better QE often show longer lifetimes. However, leaving that factor aside as perhaps an overall material and sample dependent scaling factor, we see an interesting systematic trend for the wavelength dependence of the QD lifetimes as we vary the compositions. Even allowing for variations in QE, QDs with higher Hg^{2+} content generally show far longer PL decay times (Figure 8). For CdTe QDs, lifetimes increased with increasing wavelength. For Hg^{2+} concentrations between 0 and 100% intermediate behavior is seen. At low concentrations, on the low wavelength side, the lifetimes increase with wavelength, reaching a peak value and then decline with further increasing wavelength. Although the lifetimes at the HgTe extremum of the composition range are somewhat longer than those of the CdTe starting material, it appears that the true limiting lifetime may be longer still. The β values for the pure HgTe QDs are >0.8 and the largest values obtained for smaller particle size aliquots during the growth were around 0.83 ($\tau = 118$ ns).

It should be pointed out that the extent of Hg/Cd alloying will not be identical for all QDs within the ensemble of particle sizes for a given sample. Inhomogeneous broadening will arise from both the size distribution (which may not change much relative to the starting CdTe batch, at least initially) and the distribution of Hg/Cd ratios within the ensemble. A further broadening factor may also be a distribution of the degree of Hg^{2+} mixing from dot to dot, i.e. how far from the QD surface the Hg^{2+} has managed to diffuse by the time the PL spectrum is measured. If the Hg^{2+} is still largely at the surface, the emission spectrum is essentially that of a core-shell CdTe QD (with CdTe core of slightly smaller diameter than the starting CdTe). Dots of a given size with higher, well mixed Hg^{2+} content will have longer wavelength luminescence than those with a lower Hg^{2+} content. So the different lifetime vs. wavelength trends on either side of the emission peak, may simply reflect the fact that the emission on the short wavelength side may be from higher Cd^{2+} content dots than on the long wavelength side. Of course the various broadening mechanisms (size distribution, compositional distribution, internal spatial distribution) are all superimposed, so it is not easy to unravel the contributions to the lifetime explicitly. In such small particles it is very difficult to get direct confirmation of the localization of the respective cations; indeed good quality images of the small mercaptoacid stabilized particles as a whole are difficult to obtain by HRTEM. The lattice constants of HgTe, CdTe and their alloys are very similar and the contrast in the electron transmission coefficients of Hg^{2+} and Cd^{2+} ions are likewise very similar making direct determination of the internal structures difficult.

4. Conclusions

We have followed the evolution of the bandgap energy, emission wavelengths, Stokes shifts and other associated optical properties of CdTe nanocrystals during ion exchange with Hg^{2+} ions to form QDs with $Cd_xHg_{(1-x)}Te$ alloy compositions. The ion exchange process is shown to reduce the fluorescence quantum efficiency initially, though this recovers markedly after the initial exchange stage. At this stage we have made no attempt to shorten this recovery process, though it may be possible to anneal the materials post-exchange to accelerate the slow interdiffusion process observed after the initial ingress of Hg^{2+} ions. The option to change both composition and particle sizes in principle allows the tuning of not just the bandgap energy, but also the relative positions of other energy levels, such as states near the top of the valence band which can have a significant effect on both lifetimes and measured ensemble quantum efficiencies.[47] Following the shifts in optical properties against time has allowed us to examine the kinetics of the exchange process. We observe an initial fast stage followed by a far slower phase attributed to intermixing of the respective cations after the faster exchange across the QD interface. The data presented here for $Cd_xHg_{(1-x)}Te$ alloy QDs are highly relevant for those seeking to optimize this material's design for optoelectronic components such as solar conversion devices, e.g., for luminescent collectors and other types of solar cells.

5. Experimental Section

Synthesis of $Cd_xHg_{(1-x)}Te$ Alloy QDs by Cationic Exchange: The CdTe QD (2.3 nm diameter) starting material was synthesised using a previously reported method,[11] but with an electrochemical source of H_2Te[32,49] rather than Al_2Te_3 as the precursor for the gas. Prior to the ion exchange experiment, the master batch of CdTe QD solution was precipitated with iso-propanol, centrifuged and re-dispersed in DI water. This removed excess un-reacted Cd^{2+} and other unwanted precursors and by-products of the CdTe growth reaction prior to the cationic exchange. The batch was then split into 8 portions and to each varying amounts of Hg^{2+} solutions (0.286 M $Hg(ClO_4)_2{\cdot}xH_2O$, complexed with 2.4 fold molar excess of mercaptopropionic acid, pH adjusted to 10.8 with 1 M NaOH(aq)) were added. Solutions were designated by the amount of Hg^{2+} (%) added relative to the original concentrations of Cd^{2+} ions in the master batch and ranged from 5% up to 500%. In practice the relative amount of Hg^{2+} actually exchanged differed, and for higher Hg^{2+} doses was significantly lower than the ratio added. The uptake of Hg^{2+} ions was time (and temperature) dependant.

Measurements and Data Analysis: Absorption spectra were measured on Cary 50 (λ_{abs} = 200–850 nm), or Shimadzu UV 3600 (λ_{abs} = 200–3200 nm) absorption spectrometers and photoluminescence (PL) spectra in the emission range from 200 nm to 850 nm were measured on a Cary Eclipse (λ_{pl} = 200–850 nm) PL spectrometer. For the IR range above 800 nm a Spectral Products monochromator, equipped with an electronically chopped high brightness 460 nm blue LED, a 700 nm order sorting filter and a ThorLabs Ge photodiode, monitored with a lock-in amplifier referenced to the chopped signal waveform was used to measure fluorescence spectra.

The quantum efficiency (QE) of the QDs in solution was determined by comparing the integrated PL intensities as a function of emission energy and absorption strengths against a Rhodamine B dye solution with known quantum yield. This can be done in a ratiometric manner[50] for the initial CdTe and for the low-*x* alloy $Cd_xHg_{(1-x)}Te$ QDs which emit at and have their absorption spectra at shorter wavelength. For the longer wavelength materials with little overlap with the dye standard, the ratio of their integrated PL intensities normalized by the linear absorption at the respective excitation intensities (i.e., a value proportional to the amount of light absorbed during PL measurements) was determined and compared with the value for the pure CdTe QD solution that was also referenced to the dye. For the IR measurements the power absorbed normalizing factor was determined by integrating across the product of the QD linear absorption spectrum and the blue LED source emission spectrum. The relative scaling factor for the IR PL spectrometer and the Cary PL spectrometer was established by comparing measurements for one material made on both instruments at wavelengths where measuring ranges of the two machines overlapped.

Time-resolved PL (TRPL) spectra were measured using a 200 ps pulsed laser diode (405 nm/2.5 MHz/1 mW) as the excitation source. The TRPL signals were dispersed using a 0.55 m spectrometer and detected using a multichannel LN_2-cooled charge-coupled device, photomultiplier tubes, and a photon-counting avalanche photodiode. The decay traces were recorded using a time-correlated single photon counting approach (Time-Harp, PicoQuant).

Elemental analysis of QDs was performed using a Perkin Elmer Optima 2100DV Inductively Coupled Plasma Optical Emission Atomic Absorption Spectrometer (ICP-AA). Samples were first precipitated with iso-propanol, dried and then digested in dilute aqua regia. The resulting ionic solutions were quantitatively diluted further as necessary for optimum instrumental sensitivity before analysis.

Supporting Information

Supporting Information is available from the Wiley Online Library or from the author.

Acknowledgments

This work was supported by the Applied Research Grants of City University of Hong Kong (9667042 and 9667067), by a grant from the Research Grants Council of the Hong Kong S.A.R, China (project CityU 102412), and by the National Science Council of Taiwan under Grant No. NSC 100-2119-M-009-003. The authors are grateful to Mr. H.H. Chan of City University's BCH department who performed the ICP-AA composition measurements.

Received: December 04, 2012
Revised: January 22, 2013

[1] X. Zhong, Y. Feng, W. Knoll, M. Han, *J. Am. Chem. Soc.* **2003**, *125*, 13559.
[2] R. E. Bailey, S. M. Nie, *J. Am. Chem. Soc.* **2003**, *125*, 7100.
[3] A. L. Pan, H. Yang, R. B. Liu, R. C. Yu, B. S. Zou, Z. L. Wang, *J. Am. Chem. Soc.* **2005**, *127*, 15692.
[4] D. H. Son, S. M. Hughes, Y. Yin, A. P. Alivisatos, *Science* **2004**, *306*, 1009.
[5] R. D. Robinson, B. Sadtler, D. O. Demchenko, C. K. Erdonmez, L.-W. Wang, A. P. Alivisatos, *Science* **2007**, *317*, 355.
[6] D. Schooss, A. Mews, A. Eychmüller, H. Weller, *Phys. Rev. B* **1994**, *49*, 17072.
[7] A. L. Rogach, M. T. Harrison, S. V. Kershaw, A. Kornowski, M. G. Burt, A. Eychmüller, H. Weller, *Phys. Status Solidi (b)* **2001**, *224*, 153.
[8] M. T. Harrison, S. V. Kershaw, A. L. Rogach, A. Kornowski, A. Eychmüller, H. Weller, *Adv. Mater.* **2000**, *12*, 123.
[9] R. Landolt-Bornstein, Numerical Data and Functional Relationships in Science and Technology, Vol. 18 in *Crystal and Solid State Physics*, Springer, Berlin **1984**.
[10] A. Rogalski, *Rep. Prog. Phys.* **2005**, *68*, 2267.
[11] A. L. Rogach, T. Franzl, T. A. Klar, J. Feldmann, N. Gaponik, V. Lesnyak, A. Shavel, A. Eychmüller, Y. P. Rakovich, J. F. Donegan, *J. Phys. Chem. C* **2007**, *111*, 14628.
[12] M. T. Harrison, S. V. Kershaw, M. G. Burt, A. L. Rogach, A. Eychmüller, H. Weller, *J. Mater. Chem.* **1999**, *9*, 2721.
[13] S. V. Kershaw, M. Harrison, A. L. Rogach, A. Kornowski, *IEEE J. Sel. Top. Quantum Electron.* **2000**, *6*, 534.
[14] S. V. Kershaw, M. Burt, M. Harrison, A. L. Rogach, H. Weller, A. Eychmüller, *Appl. Phys. Lett.* **1999**, *75*, 1694.
[15] S. Taniguchi, M. Green, *J. Mater. Chem.* **2011**, *21*, 11592.
[16] S. Taniguchi, M. Green, T. Lim, *J. Am. Chem. Soc.* **2011**, *133*, 3328.
[17] V. Lesnyak, A. Lutich, N. Gaponik, M. Grabolle, A. Plotnikov, U. Resch-Genger, A. Eychmüller, *J. Mater. Chem.* **2009**, *19*, 9147.
[18] H. Sun, H. Zhang, J. Ju, J. Zhang, G. Qian, C. Wang, B. Yang, Z. Y. Wang, *Chem. Mater.* **2008**, *20*, 6764.
[19] G. D. Moon, S. Ko, Y. Min, J. Zeng, Y. Xia, U. Jeong, *Nano Today* **2011**, *6*, 186.
[20] J. Yang, Y. L. Zhou, S. L. Zheng, X. F. Liu, X. H. Qiu, Z. Y. Tang, R. Song, Y. J. He, C. W. Ahn, J. W. Kim, *Chem. Mater.* **2009**, *21*, 3177.
[21] A. Kongkanand, K. Tvrdy, K. Takechi, M. Kuno, P. V. Kamat, *J. Am. Chem. Soc.* **2008**, *130*, 4007.
[22] J. Bomm, A. Büchtemann, A. J. Chatten, R. Bose, D. J. Farrell, N. L. A. Chan, Y. Xiao, L. H. Slooff, T. Meyer, A. Meyer, W. G. J. H. M. van Sark, R. Koole, *Sol. Energy Mater. Sol. Cells* **2011**, *95*, 2087.
[23] B. C. Rowan, L. R. Wilson, B. S. Richards, *IEEE J. Sel. Top. Quantum Electron.* **2008**, *14*, 1312.
[24] A. L. Rogach, M. Ogris, *Curr. Opin. Mol. Therap.* **2010**, *12*, 331.
[25] C. L. Amiot, S. Xu, S. Liang, L. Pan, J. X. Zhao, *Sensors* **2008**, *8*, 3082.
[26] J. Baars, F. Sorger, *Solid State Commun.* **1972**, *10*, 875.
[27] The effective mass curve was calculated from electron effective masses from:J. L. Schmit, *J. Appl. Phys.* **1970**, *41*, 2876, assuming a constant hole effective mass of 0.44 m_o.
[28] G. A. Antcliffe, *Phys. Rev. B.* **1970**, *2*, 345.
[29] J. Pérez-Condea, A. K. Bhattacharjeeb, *Solid State Commun.* **1999**, *110*, 259.
[30] Y. Nemirowsky, E. J. Finkmann, *Appl. Phys.* **1979**, *50*, 8107.
[31] M. T. Harrison, S. V. Kershaw, M. G. Burt, A. Eychmüller, H. Weller, A. L. Rogach, *Mater. Sci. Eng. B* **2000**, *69-70*, 355.
[32] M. V. Kovalenko, E. Kaufmann, D. Pachinger, J. Roither, M. Huber, J. Stangl, G. Hesser, F. Schäffler, W. Heiss, *J. Am. Chem. Soc.* **2006**, *128*, 3516.
[33] J. S. Kamal, A. Omari, K. Van Hoecke, Q. Zhao, A. Vantomme, F. Vanhaecke, R. K. Capek, Z. Hens, *J. Phys. Chem. C* **2012**, *116*, 5049.
[34] I. Moreels, K. Lambert, D. De Muynck, F. Vanhaecke, D. Poelman, J. C. Martins, G. Allan, Z. Heger, *Chem. Mater.* **2007**, *19*, 6101.
[35] I. Moreels, K. Lambert, D. Smeets, D. De Muynck, T. Nollet, J. C. Martins, F. Vanhaecke, A. Vantomme, C. Delerue, G. Allan, Z. Hens, *ACS Nano* **2009**, *3*, 3023.
[36] E. Lhuillier, S. Keuleyan, P. Guyot-Sionnest, *Nanotechnology* **2012**, *23*, 175705.
[37] M. Protière, P. Reiss, *Small* **2007**, *3*, 399.
[38] J. E. Bernard, A. Zunger, *Phys. Rev. B* **1986**, *34*, 5992.
[39] S.-H. Wei, S. B. Zhang, A. Zunger, *J. Appl. Phys.* **2000**, *87*, 1304.
[40] B. J. Beberwyck, A. P. Alivisatos, *J. Am. Chem. Soc.* **2012**, *134*, 19977.
[41] W. W. Yu, L. Qu, W. Guo, X. Peng, *Chem. Mater.* **2003**, *15*, 2854.
[42] K. Huang, A. Rhys, *Proc. R. Soc. London, Ser. A* **1950**, *204*, 406.
[43] J. Garcia Solè, L. E. Bausà, D. Jacque, *An Introduction to the Optical Spectroscopy of Inorganic Solids*, Wiley, Hoboken, NJ **2005**.
[44] V. Dzhagan, M. Ya. Valakh, J. Kolny-Olesiak, I. Lokteva, D. R. T. Zahn, *Appl. Phys. Lett.* **2009**, *94*, 243101.
[45] R. Dornhaus, G. Nimtz, The Properties and Applications of the $Hg_{1-x}Cd_xTe$ Alloy System, in *Springer Tracts in Modern Physics*, Springer-Verlag, Berlin **1976**, Vol. 78.
[46] P. K. Jain, B. J. Beberwyck, L.-K. Fong, M. J. Polking, A. P. Alivisatos, *Angew. Chem.* **2012**, *124*, 2437, P. K. Jain, B. J. Beberwyck, L.-K. Fong, M. J. Polking, A. P. Alivisatos, *Angew. Chem. Int. Ed.* **2012**, *51*, 2387.
[47] A. F. van Driel, G. Allan, C. Delerue, P. Lodahl, W. L. Vos, D. Vanmaekelbergh, *Phys. Rev. Lett.* **2005**, *95*, 236804.
[48] D. V. Talapin, A. L. Rogach, E. V. Shevchenko, A. Kornowski, M. Haase, H. Weller, *J. Am. Chem. Soc.* **2002**, *124*, 5782.
[49] W. Hempel, M. G. Weber, *Z. Anorg. Chem.* **1912**, *77*, 48.
[50] M. Grabolle, M. Spieles, V. Lesnyak, N. Gaponik, A. Eychmüller, U. Resch-Genger, *Anal. Chem.* **2009**, *81*, 6285.